Detecting, anticipating, and predicting critical transitions in spatially extended systems

Frank Kwasniok

Citation: Chaos **28**, 033614 (2018); doi: 10.1063/1.5022189
View online: https://doi.org/10.1063/1.5022189
View Table of Contents: http://aip.scitation.org/toc/cha/28/3
Published by the American Institute of Physics

Detecting, anticipating, and predicting critical transitions in spatially extended systems

Frank Kwasniok[a)]
College of Engineering, Mathematics and Physical Sciences, University of Exeter, North Park Road, Exeter EX4 4QF, United Kingdom

(Received 11 January 2018; accepted 2 March 2018; published online 22 March 2018)

A data-driven linear framework for detecting, anticipating, and predicting incipient bifurcations in spatially extended systems based on principal oscillation pattern (POP) analysis is discussed. The dynamics are assumed to be governed by a system of linear stochastic differential equations which is estimated from the data. The principal modes of the system together with corresponding decay or growth rates and oscillation frequencies are extracted as the eigenvectors and eigenvalues of the system matrix. The method can be applied to stationary datasets to identify the least stable modes and assess the proximity to instability; it can also be applied to nonstationary datasets using a sliding window approach to track the changing eigenvalues and eigenvectors of the system. As a further step, a genuinely nonstationary POP analysis is introduced. Here, the system matrix of the linear stochastic model is time-dependent, allowing for extrapolation and prediction of instabilities beyond the learning data window. The methods are demonstrated and explored using the one-dimensional Swift-Hohenberg equation as an example, focusing on the dynamics of stochastic fluctuations around the homogeneous stable state prior to the first bifurcation. The POP-based techniques are able to extract and track the least stable eigenvalues and eigenvectors of the system; the nonstationary POP analysis successfully predicts the timing of the first instability and the unstable mode well beyond the learning data window. *Published by AIP Publishing.* https://doi.org/10.1063/1.5022189

Critical transitions or tipping points are described as sudden, possibly irreversible, disproportionate changes in the output of a complex system in response to small changes in the input. Such abrupt shifts have been observed, e.g., in ecosystems, the climate system, financial markets, or biomedical applications. There has been much research in recent years devoted to extracting from time series data early-warning signals preceding critical transitions. In cases where the transition is due to a bifurcation, two generic features are often found when approaching the bifurcation: an increasingly slow recovery of the system from noisy perturbations, known as critical slowing down, as well as an increasing variance of the fluctuations around the (quasi-)equilibrium state.

In this paper, we discuss data-based detection, anticipation, and prediction of bifurcation-induced critical transitions in spatially extended systems. A linear framework of nonstationary dynamical modelling is adopted to identify and track the characteristic modes of the system with corresponding decay/growth rates and oscillation frequencies. Unlike most previous work, we also discuss genuine prediction of critical transitions (rather than just detection and anticipation) by extrapolation of the dynamical model beyond the learning data window.

I. INTRODUCTION

Many complex dynamical systems may experience drastic sudden changes in their behavior, so-called critical transitions or tipping points. Often, these are due to bifurcations,[1] that is, there is a slow drift of a system parameter toward a local bifurcation point. It is desirable to find early-warning signs based on measured time series from the system to indicate whether a critical transition is imminent in order to avoid or mitigate its impact. There has been tremendous progress in recent years in identifying early-warning signs for approaching bifurcations in noisy systems. The most generic and widely used early-warning signs are increasing autocorrelation (critical slowing down)[2,3] and increasing variance.[4,5] Other indicators are trends in skewness[6] and quasi-stationary probability densities and their modality.[7,8] A more quantitative and dynamically motivated approach lies in deriving a nonstationary model from data and then propagating it beyond the learning data window to study its projected future behaviour.[9–13]

So far, most of the data-based work on critical transitions refers to univariate time series. The additional data in a multivariate setting can be expected to improve existing early-warning signs and open the possibility to discover new ones. A multivariate analysis based on tracking the (complex) eigenvalues of the Jacobian matrix of the system reconstructed from data has been proposed recently.[14] For spatially extended systems, early-warning signs of critical transitions discussed in the literature include increasing autocorrelation,[15] spatial correlation,[16] spatial variance, and skewness[17,18] as well as the patchiness of states.[19] A mathematically rigorous analysis of stochastic partial differential equations approaching bifurcations has been performed recently focusing on analytically deriving basic scaling laws of the covariance operator for linear stochastic partial

a)Electronic mail: F.Kwasniok@exeter.ac.uk

differential equations and comparing the results to numerical simulations of fully nonlinear problems.[20]

This paper transfers the approach of nonstationary dynamical modelling to spatially extended systems. The dynamics are approximated by a system of linear stochastic differential equations which is identified from data using statistical estimation techniques. The least stable modes of the system are tracked and instabilities are predicted based on analysis of the eigenvalues and eigenvectors of the system matrix.

The method is meant to be a generic technique of critical transition analysis for pattern-forming spatial systems. Possible applications are vegetation patterns in theoretical ecology and the meridional overturning circulation or the El Niño–Southern Oscillation phenomenon in climate science.

This paper is organized as follows: The methodology is discussed in Sec. II. Section III introduces the stochastic Swift-Hohenberg equation used here as an example system and details its properties and its numerical solution. The results are presented in Sec. IV. The paper finishes with some discussion and concluding remarks in Sec. V.

II. METHODOLOGY

The methodology builds on principal oscillation pattern (POP) analysis, a technique proposed in the field of climate science.[21,22] A similar technique termed dynamic mode decomposition has been introduced in the field of engineering fluid dynamics.[23] For completeness, POP analysis is here briefly recapitulated. It is then put into a nonstationary context using a sliding window approach which has not been done previously. The main methodological contribution of the present paper lies in introducing a genuinely nonstationary POP analysis.

We consider a complex, spatially extended system described by a D-dimensional state vector $\mathbf{X} = (X_1,\ldots, X_D)^{\mathrm{T}}$. A time series of the system, $\{\mathbf{X}_0,\ldots, \mathbf{X}_N\}$, is available with $\mathbf{X}_n = \mathbf{X}(t_n) = (X_{1,n},\ldots,X_{D,n})^{\mathrm{T}}$. The time series may be evenly or unevenly sampled; the sampling interval is $\delta t_n = t_{n+1} - t_n$. The dataset may originate from observations with the components of the state vector representing measurements at different locations; or it may originate from numerical simulation of a high-dimensional, deterministic, or stochastic dynamical system. In the latter case, the system may be an infinite-dimensional partial differential equation; the components of the state vector $\mathbf{X}$ then are grid point values from a finite-difference discretization or Fourier coefficients from a spectral discretization.

A. Stationary data

We first assume that the dataset stems from a stationary system. The stationary analysis refers to detection of critical transitions or detection of the proximity of a system to a transition threshold.

1. Dimension reduction using principal component analysis

Prior to the POP analysis, the dimension of the dataset is reduced via principal component analysis,[24] also referred to as proper orthogonal decomposition (POD) or empirical orthogonal function (EOF) analysis. The mean state of the system $\langle\mathbf{X}\rangle$ is given as the sample mean of the dataset

$$\langle\mathbf{X}\rangle = \frac{1}{N+1}\sum_{n=0}^{N}\mathbf{X}_n. \tag{1}$$

The dataset is projected onto K modes, with $K \ll D$, which account for most of the variance of the fluctuations around the mean state. More precisely, we seek an expansion

$$\mathbf{X}_n = \langle\mathbf{X}\rangle + \sum_{j=1}^{K} y_{j,n}\,\mathbf{e}_j, \tag{2}$$

with $y_{j,n} = \mathbf{e}_j^{\mathrm{T}}\mathbf{M}(\mathbf{X}_n - \langle\mathbf{X}\rangle)$ such that the error function

$$J = \frac{1}{N}\sum_{n=0}^{N-1}\left(\mathbf{X}_n - \langle\mathbf{X}\rangle - \sum_{j=1}^{K} y_{j,n}\,\mathbf{e}_j\right)^{\mathrm{T}} \times \mathbf{M}\left(\mathbf{X}_n - \langle\mathbf{X}\rangle - \sum_{j=1}^{K} y_{j,n}\,\mathbf{e}_j\right) \tag{3}$$

is minimized with respect to the modes $\{\mathbf{e}_j\}_{j=1}^{K}$ subject to the orthonormality constraints

$$\mathbf{e}_j^{\mathrm{T}}\mathbf{M}\mathbf{e}_k = \delta_{jk}, \tag{4}$$

where δ_{jk} denotes the Kronecker delta symbol. The symmetric, positive definite matrix $\mathbf{M}$ is the metric in which the error is measured. It may often be equal to the identity matrix corresponding to the Euclidian norm; but, for example, in the case of a fluid system, it may be different and correspond to an energy or enstrophy norm. For any K, the solution to the optimization problem is given by the eigenvectors corresponding to the K largest eigenvalues of the eigenvalue problem

$$\mathbf{\Gamma}\mathbf{M}\mathbf{e}_j = \mu_j\mathbf{e}_j, \tag{5}$$

where $\mathbf{\Gamma}$ is the covariance matrix of the fluctuations given by

$$\mathbf{\Gamma} = \frac{1}{N}\sum_{n=0}^{N-1}(\mathbf{X}_n - \langle\mathbf{X}\rangle)(\mathbf{X}_n - \langle\mathbf{X}\rangle)^{\mathrm{T}}. \tag{6}$$

The principal components are uncorrelated and the eigenvalue μ_j gives the variance accounted for by the mode $\mathbf{e}_j$

$$\frac{1}{N}\sum_{n=0}^{N-1} y_{j,n}y_{k,n} = \mu_j\delta_{jk}. \tag{7}$$

The minimum of the cost function is $J = \sum_{j=K+1}^{D}\mu_j$. In order to solve the eigenvalue problem of Eq. (5), it is most convenient to solve the symmetric, positive definite eigenvalue problem $\mathbf{M}^{1/2}\mathbf{\Gamma}\mathbf{M}^{1/2}\hat{\mathbf{e}}_j = \mu_j\hat{\mathbf{e}}_j$ with the same eigenvalues μ_j and then obtain the eigenvectors as $\mathbf{e}_j = \mathbf{M}^{-1/2}\hat{\mathbf{e}}_j$.

The dataset is reduced to the time series of the principal components, $\{\mathbf{y}_0,\ldots,\mathbf{y}_N\}$, with $\mathbf{y}_n = \mathbf{y}(t_n) = (y_{1,n},\ldots,y_{K,n})^{\mathrm{T}}$.

We remark that a dimension reduction of the dataset prior to the POP analysis is often convenient if the dimension

D is very large, but it is not principally necessary. The POP analysis described below could also be performed directly on the anomaly time series $\{\mathbf{X}_0 - \langle\mathbf{X}\rangle, \ldots, \mathbf{X}_N - \langle\mathbf{X}\rangle\}$.

2. Principal oscillation patterns (POPs)

The dynamics of the principal components are approximated by a system of linear stochastic differential equations

$$\dot{y}_j = \sum_{k=1}^{K} A_{jk} y_k + \sum_{k=1}^{K} \sigma_{jk} \eta_k, \tag{8}$$

where η_k are white independent standard Gaussian processes. Generically, the system matrix $\mathbf{A}$ can be diagonalized as $\mathbf{V}^{-1}\mathbf{A}\mathbf{V} = \mathrm{diag}(\lambda_1, \ldots, \lambda_K)$ where the scalars $\{\lambda_j\}_{j=1}^{K}$ and the matrix $\mathbf{V}$ are generally complex. The j-th column of $\mathbf{V}$, $\mathbf{v}_j$, is an eigenvector of the system matrix $\mathbf{A}$ with eigenvalue λ_j

$$\mathbf{A}\mathbf{v}_j = \lambda_j \mathbf{v}_j. \tag{9}$$

The eigenvalues are ordered by non-increasing real part. The linear transformation $\mathbf{z} = \mathbf{V}^{-1}\mathbf{y}$ corresponds to an expansion of the state vector as

$$\mathbf{X} = \langle\mathbf{X}\rangle + \sum_{j=1}^{K} z_j \, \mathbf{p}_j, \tag{10}$$

with $\mathbf{p}_j = \sum_{k=1}^{K} V_{kj}\mathbf{e}_k$ where the dynamics of the expansion coefficients z_j follow the decoupled equations:

$$\dot{z}_j = \lambda_j z_j + \sum_{k=1}^{K} \hat{\sigma}_{jk} \eta_k, \tag{11}$$

with $\hat{\sigma}_{jk} = \sum_{l=1}^{K} (\mathbf{V}^{-1})_{jl}\sigma_{lk}$. The modes $\{\mathbf{p}_j\}_{j=1}^{K}$ are the principal oscillation patterns (POPs) of the system. The dynamics of the mode $\mathbf{p}_j$, characterized by the eigenvalue

$$\lambda_j = \nu_j + i\omega_j, \tag{12}$$

correspond to an oscillation with frequency ω_j (period $2\pi/\omega_j$) and an e-folding time of growth or decay of $1/|\nu_j|$. The POP modes come as single, real modes (with zero frequency) or as pairs of complex conjugate modes. The expansion coefficients $\{z_j\}_{j=1}^{K}$ generally cannot be assumed to be uncorrelated as the driving stochastic terms are correlated.

The system matrix $\mathbf{A}$ is estimated from data. Two possible estimation techniques are available. One can discretize the model of Eq. (8) using the Euler-Maruyama scheme[28] with step sizes taken equal to the sampling intervals

$$y_{j,n+1} = y_{j,n} + \delta t_n \sum_{k=1}^{K} A_{jk} y_{k,n} + \sqrt{\delta t_n} \sum_{k=1}^{K} \sigma_{jk} \eta_{k,n}, \tag{13}$$

corresponding to the data log-likelihood function

$$\log p(\mathbf{y}_1, \ldots, \mathbf{y}_N | \mathbf{y}_0) = \sum_{n=0}^{N-1} \log p(\mathbf{y}_{n+1} | \mathbf{y}_n), \tag{14}$$

with the Gaussian transition probability density

$$p(\mathbf{y}_{n+1} | \mathbf{y}_n) \sim \mathcal{N}(\mathbf{y}_n + \delta t_n \mathbf{A}\mathbf{y}_n, \delta t_n \mathbf{D}), \tag{15}$$

where the diffusion matrix $\mathbf{D}$ is given as $D_{jk} = \sum_{l=1}^{K} \sigma_{jl}\sigma_{kl}$. The maximum likelihood estimator for the system matrix $\mathbf{A}$ is then the least-squares estimator given as

$$\mathbf{A} = \mathbf{G}_1 \mathbf{G}_0^{-1}, \tag{16}$$

with the covariance matrices

$$\mathbf{G}_0 = \frac{1}{N} \sum_{n=0}^{N-1} \delta t_n \mathbf{y}_n \mathbf{y}_n^{\mathrm{T}}, \tag{17}$$

$$\mathbf{G}_1 = \frac{1}{N} \sum_{n=0}^{N-1} (\mathbf{y}_{n+1} - \mathbf{y}_n) \mathbf{y}_n^{\mathrm{T}}. \tag{18}$$

The Euler-Maruyama discretization is consistent only in the limit of infinitesimally small sampling intervals δt_n. For finite sampling intervals, the estimator is biased even in the limit of large N. In practice, the estimator can be expected to be reliable for POP modes for which the sampling intervals are very small compared with the growth/decay timescale and the period of oscillation.

In the case of evenly sampled data ($\delta t_n = \delta t$), there is an alternative way of estimating the system matrix $\mathbf{A}$. The discrete linear stochastic model

$$y_{j,n+1} = \sum_{k=1}^{K} B_{jk} y_{k,n} + \sum_{k=1}^{K} \rho_{jk} \eta_{k,n}, \tag{19}$$

is equivalent to the continuous model of Eq. (8), sampled at intervals δt, if the system matrices $\mathbf{A}$ and $\mathbf{B}$ are related as

$$\mathbf{A} = \frac{1}{\delta t} \log \mathbf{B}. \tag{20}$$

The discrete model has transition probability density

$$p(\mathbf{y}_{n+1} | \mathbf{y}_n) \sim \mathcal{N}(\mathbf{B}\mathbf{y}_n, \mathbf{R}), \tag{21}$$

with noise covariance matrix $\mathbf{R}$ given by $R_{jk} = \sum_{l=1}^{K} \rho_{jl}\rho_{kl}$. The maximum likelihood estimator for the system matrix $\mathbf{B}$ is the least-squares estimator given by

$$\mathbf{B} = \mathbf{C}_1 \mathbf{C}_0^{-1}, \tag{22}$$

with the covariance matrices

$$\mathbf{C}_0 = \frac{1}{N} \sum_{n=0}^{N-1} \mathbf{y}_n \mathbf{y}_n^{\mathrm{T}}, \tag{23}$$

$$\mathbf{C}_1 = \frac{1}{N} \sum_{n=0}^{N-1} \mathbf{y}_{n+1} \mathbf{y}_n^{\mathrm{T}}. \tag{24}$$

In the case of a dimension reduction with principal components, we have $\mathbf{C}_0 = \mathrm{diag}(\mu_1, \ldots, \mu_K)$ by virtue of Eq. (7). Then $\mathbf{A}$ is calculated from Eq. (20) and its eigenvalues and eigenvectors analyzed as before. This estimation procedure is asymptotically unbiased in the limit of large N regardless of the sampling interval δt.

There are also maximum likelihood estimates for the diffusion matrix **D** and the noise covariance matrix **R** as well as an expression relating them for evenly sampled data, but this is less relevant here, as we focus on the system matrix in the present context.

B. Nonstationary data

Two methods for analyzing nonstationary data are discussed: a sliding-window approach where the system is regarded as stationary over a certain time window, and an approach which models the nonstationarity explicitly.

1. Sliding window approach

In the sliding window approach, at each time instant t, the time window $[t - T_\mathrm{w}, t]$ is considered and the system is regarded as stationary in that window. A POP analysis is performed as described above using all of the data points in the interval $[t - T_\mathrm{w}, t]$. The eigenvalues and eigenvectors of the system matrix **A** are assigned to the time t. The size of the sliding window, T_w, is a parameter of the method. Different values of T_w should be used in the analysis to check for robustness of the results. Generally, this approach can be expected to lag behind the true stability properties of the system as always data from the past are used in the analysis.

The sliding window approach corresponds to anticipation of critical transitions, as it allows to track the linear stability properties of the system over time; it cannot be termed a prediction, as it has no provision to extrapolate into the future and forecast the timing of the transition.

2. Nonstationary POP analysis

In the nonstationary POP analysis, the nonstationarity of the system matrix is modeled explicitly and inferred from data. The technique allows for genuine prediction of the timing and nature of critical transitions. Again, a system of linear stochastic differential equations is assumed

$$\dot{y}_j = \sum_{k=1}^{K} A_{jk}(t) y_k + \sum_{k=1}^{K} \sigma_{jk} \eta_k, \tag{25}$$

but now with a time-dependent system matrix $\mathbf{A}(t)$. It is represented as

$$\mathbf{A}(t) = \sum_{j=0}^{S} \beta_j(t) \mathbf{A}_j, \tag{26}$$

where $\beta_j(t)$ are prescribed basis functions. We always set $\beta_0(t) = 1$ for the stationary part of the system. The basis functions $\beta_j(t)$ for $j > 0$ might be trends (polynomial or other) or trigonometric functions to model periodicities. The model parameters $\{\mathbf{A}_j\}_{j=0}^{S}$ are estimated from data in a learning data window. Equation (26) then allows to reconstruct the system matrix anywhere in the learning data window as well as to predict it for future times by extrapolating beyond the learning data window.

There are again two ways for parameter estimation. One can discretize the nonstationary model of Eq. (25) using the Euler-Maruyama scheme with step sizes equal to the sampling intervals. The maximum likelihood estimate for the parameters is then the least-squares estimator given by

$$(\, \mathbf{A}_0 \quad \mathbf{A}_1 \quad \cdots \quad \mathbf{A}_S \,) = \mathbf{H}_1 \mathbf{H}_0^{-1}, \tag{27}$$

where

$$\mathbf{H}_0 = \begin{pmatrix} \mathbf{H}_{0,0,0} & \mathbf{H}_{0,0,1} & \cdots & \mathbf{H}_{0,0,S} \\ \mathbf{H}_{0,1,0} & \mathbf{H}_{0,1,1} & \cdots & \mathbf{H}_{0,1,S} \\ \vdots & \vdots & \vdots & \vdots \\ \mathbf{H}_{0,S,0} & \mathbf{H}_{0,S,1} & \cdots & \mathbf{H}_{0,S,S} \end{pmatrix}, \tag{28}$$

$$\mathbf{H}_1 = (\, \mathbf{H}_{1,0} \quad \mathbf{H}_{1,1} \quad \cdots \quad \mathbf{H}_{1,S} \,), \tag{29}$$

with the covariance matrices

$$\mathbf{H}_{0,j,k} = \frac{1}{N} \sum_{n=0}^{N-1} \delta t_n \beta_{j,n} \beta_{k,n} \mathbf{y}_n \mathbf{y}_n^\mathrm{T}, \tag{30}$$

$$\mathbf{H}_{1,j} = \frac{1}{N} \sum_{n=0}^{N-1} \beta_{j,n} (\mathbf{y}_{n+1} - \mathbf{y}_n) \mathbf{y}_n^\mathrm{T}, \tag{31}$$

and $\beta_{j,n} = \beta_j(t_n)$.

In the case of equally sampled data, one can define a discrete linear stochastic model as in Eq. (19), but now with the time-dependent system matrix

$$\mathbf{B}(t) = \sum_{j=0}^{S} \beta_j(t) \mathbf{B}_j. \tag{32}$$

The maximum likelihood estimate for the parameters is then the least-squares estimator given by

$$(\, \mathbf{B}_0 \quad \mathbf{B}_1 \quad \cdots \quad \mathbf{B}_S \,) = \mathbf{F}_1 \mathbf{F}_0^{-1}, \tag{33}$$

where

$$\mathbf{F}_0 = \begin{pmatrix} \mathbf{F}_{0,0,0} & \mathbf{F}_{0,0,1} & \cdots & \mathbf{F}_{0,0,S} \\ \mathbf{F}_{0,1,0} & \mathbf{F}_{0,1,1} & \cdots & \mathbf{F}_{0,1,S} \\ \vdots & \vdots & \vdots & \vdots \\ \mathbf{F}_{0,S,0} & \mathbf{F}_{0,S,1} & \cdots & \mathbf{F}_{0,S,S} \end{pmatrix}, \tag{34}$$

$$\mathbf{F}_1 = (\, \mathbf{F}_{1,0} \quad \mathbf{F}_{1,1} \quad \cdots \quad \mathbf{F}_{1,S} \,), \tag{35}$$

with the covariance matrices

$$\mathbf{F}_{0,j,k} = \frac{1}{N} \sum_{n=0}^{N-1} \beta_{j,n} \beta_{k,n} \mathbf{y}_n \mathbf{y}_n^\mathrm{T}, \tag{36}$$

$$\mathbf{F}_{1,j} = \frac{1}{N} \sum_{n=0}^{N-1} \beta_{j,n} \mathbf{y}_{n+1} \mathbf{y}_n^\mathrm{T}. \tag{37}$$

The matrix $\mathbf{B}(t)$ can be reconstructed and predicted for any time t from Eq. (32) and the corresponding matrix $\mathbf{A}(t)$ calculated via Eq. (20).

We remark that, unlike in the stationary case, the two expansions of Eqs. (26) and (32) with the same value of S

and the same choice of nonstationary basis functions $\{\beta_j(t)\}_{j=1}^{S}$ are not exactly equivalent, as the relationship between $\mathbf{A}(t)$ and $\mathbf{B}(t)$ is nonlinear. But a Taylor expansion of $\mathbf{B} = \exp(\delta t \mathbf{A})$ shows that the difference is very small provided that δt is not very large and the nonstationarity of the system is relatively slow.

The number of nonstationary basis functions, S, is a hyperparameter of the method and determines the overall complexity of the model. It can be determined using standard likelihood-based model selection techniques such as information criteria or likelihood cross-validation. The number of parameters here increases quite rapidly with increasing S, producing the danger of overfitting. Often, one might just model a linear trend, that is, $S=1$ and $\mathbf{A}(t)=\mathbf{A}_0+t\mathbf{A}_1$ or $\mathbf{B}(t)=\mathbf{B}_0+t\mathbf{B}_1$.

3. Detrending

Also, the nonstationary POP model is formulated as an anomaly model. Prior to the analysis and also prior to the dimension reduction, the raw data are detrended, in line with standard practice in critical transition analysis. This can be done using a polynomial trend model (linear, quadratic, etc.), a local polynomial trend model or a nonparametric technique such as a kernel smoother.

III. THE STOCHASTIC SWIFT-HOHENBERG EQUATION

A. The deterministic model system

As an example of a pattern-forming spatially extended system to explore the methodology, the one-dimensional real Swift-Hohenberg equation,[25,26] here augmented with a dispersion term,[27] is used

$$\frac{\partial u}{\partial t} = ru + s\frac{\partial^3 u}{\partial x^3} - \left(1+\frac{\partial^2}{\partial x^2}\right)^2 u - u^3. \tag{38}$$

The model is considered on the domain $\mathcal{I}=[0,L]$ subject to periodic boundary conditions: $u(0,t)=u(L,t)$ for all t. In the absence of dispersion ($s=0$), the Swift-Hohenberg equation has variational structure[26] and admits only stationary attractors. With dispersion, the spatial reflection symmetry is broken[27] and the model admits, e.g., travelling wave solutions.

We introduce the complex scalar product

$$(g,h) = \int_0^L g^*(x)h(x)\,dx \tag{39}$$

for two functions $g(x)$ and $h(x)$, where the asterisk denotes the complex conjugate.

B. Linear analysis

The Swift-Hohenberg equation can be written as

$$\frac{\partial u}{\partial t} = \mathcal{L}u + \mathcal{N}(u), \tag{40}$$

with the nonlinear operator $\mathcal{N}(u)=-u^3$ and the linear operator $\mathcal{L}=\mathcal{L}^+ + \mathcal{L}^-$, consisting of a self-adjoint part $\mathcal{L}^+ = rI - (1+\partial^2/\partial x^2)^2$ and a skew-symmetric part $\mathcal{L}^- = s\partial^3/\partial x^3$. The linear operator $\mathcal{L}$ on the domain $\mathcal{I}$ with periodic boundary conditions has eigenfunctions

$$\phi_k(x) = \frac{1}{\sqrt{L}}\exp\left(i\frac{2\pi k x}{L}\right), \tag{41}$$

with

$$\mathcal{L}\phi_k = \alpha_k \phi_k, \tag{42}$$

where the eigenvalues are given as

$$\alpha_k = r - \left(1-\frac{4\pi^2 k^2}{L^2}\right)^2 - s\frac{8\pi^3 k^3}{L^3}i, \tag{43}$$

for $k \in \mathcal{Z}$. The eigenfunctions form an orthonormal set

$$(\phi_k, \phi_l) = \delta_{kl}. \tag{44}$$

In the case of no dispersion ($s=0$), the linear operator $\mathcal{L}$ is self-adjoint, the eigenvalues are real and for $k\neq 0$, there are two orthogonal eigenfunctions with the same eigenvalue which could be chosen real as cos and sin modes.

For simplicity, we assume that the system size L is an integer multiple of 2π. For $r<0$, the homogeneous solution $u=0$ is linearly stable as $\mathrm{Re}(\alpha_k)<0$ for all k. At $r=0$, the critical wavenumber $k_c = \pm L/2\pi$ becomes unstable; for $s=0$, there is a Turing bifurcation to a stationary wave pattern; for $s\neq 0$, there is a Hopf bifurcation to a traveling wave pattern.

C. Stochastic forcing

In order to study the dynamics of fluctuations around the homogeneous state $u=0$ prior to the first bifurcation, the Swift-Hohenberg model is augmented with stochastic forcing

$$\frac{\partial u}{\partial t} = \mathcal{L}u + \mathcal{N}(u) + \sigma\xi(x,t). \tag{45}$$

For simplicity, we restrict ourselves to additive noise here. The noise standard deviation is given by the parameter σ. The noise process $\xi(x,t)$ is a Gaussian process specified by the separable covariance function

$$\langle \xi(x,t)\xi(x',t')\rangle = C_{\mathrm{tem}}(t,t')C_{\mathrm{sp}}(x,x'), \tag{46}$$

with the temporal correlation function C_{tem} and the spatial correlation function C_{sp}. We here assume, as in Ref. 20, the noise to be white in time, that is,

$$C_{\mathrm{tem}}(t,t') = \delta(t-t'), \tag{47}$$

and the spatial correlation function is specified as

$$C_{\mathrm{sp}}(x,x') = \exp\left[-(x-x')^2/c^2\right]. \tag{48}$$

The parameter c defines the spatial correlation length. In the limit $c\to 0$, we have spatially white noise, that is, $C_{\mathrm{sp}}(x,x') = \delta(x-x')$.

D. Spatial discretization

The stochastic partial differential equation is discretized in space using a finite-difference scheme. An equally spaced mesh is introduced as $(x_0, x_1, \ldots, x_M)$ where $x_j = j\Delta x$ with mesh size $\Delta x = L/M$. The function u is discretized as $\mathbf{u} = (u_0, u_1, \ldots, u_{M-1})$ with $u_j = u(x_j)$. We arrive at the system of stochastic ordinary differential equations

$$\dot{u}_j = f_j(\mathbf{u}) + \sigma\xi_j; \quad j = 0, \ldots, M-1. \tag{49}$$

Using central differencing operators, the function f_j is given by

$$\begin{aligned} f_j(\mathbf{u}) = (r-1)u_j + s\frac{u_{j+2} - 2u_{j+1} + 2u_{j-1} - u_{j-2}}{2(\Delta x)^3} \\ - 2\frac{u_{j+1} - 2u_j + u_{j-1}}{(\Delta x)^2} \\ - \frac{u_{j+2} - 4u_{j+1} + 6u_j - 4u_{j-1} + u_{j-2}}{(\Delta x)^4} - u_j^3, \end{aligned} \tag{50}$$

with $u_{-2} = u_{M-2}$, $u_{-1} = u_{M-1}$, $u_M = u_0$ and $u_{M+1} = u_1$ from the periodic boundary condition. The scheme is of second-order accuracy.

The discrete counterpart of the scalar product of Eq. (39) is

$$(g, h) = \Delta x \sum_{j=0}^{M-1} g^*(x_j)h(x_j), \tag{51}$$

using the trapezoidal integration scheme. The metric $\mathbf{M}$ for the principal component analysis is a diagonal matrix defined by $M_{jk} = \Delta x\delta_{jk}$.

E. Time integration

In view of the severe stiffness of the Swift-Hohenberg model already at moderate resolutions, the system is integrated in time using the implicit Euler-Maruyama scheme[28]

$$u_j^{n+1} = u_j^n + f_j(\mathbf{u}^{n+1})\Delta t + \sigma\sqrt{\Delta t}\,\xi_j^n. \tag{52}$$

The scheme is unconditionally stable and of first-order accuracy. In order to advance the solution to the next time step, the system of nonlinear equations

$$G_j(\mathbf{u}^{n+1}) = u_j^{n+1} - f_j(\mathbf{u}^{n+1})\Delta t - u_j^n - \sigma\sqrt{\Delta t}\,\xi_j^n = 0, \tag{53}$$

for $j = 0, \ldots, M-1$ needs to be solved for $\mathbf{u}^{n+1}$. This is done using the Newton-Raphson method. A close first guess for $\mathbf{u}^{n+1}$ to start the iteration can be generated by the deterministic explicit Euler scheme as $u_j^{n+1} = u_j^n + f_j(\mathbf{u}^n)\Delta t$. The Jacobian matrix of $\mathbf{G} = (G_0, \ldots, G_{M-1})$ with respect to $\mathbf{u}^{n+1}$ is highly sparse which could be exploited to considerably speed up the time integration.

In the case of no spatial correlation, the variables ξ_j^n are independent standard Gaussian noises. A method for generating a noise field $\xi(x_j, t)$ which is colored in space with given correlation function (and white in time) has been described in the literature[29] and also a numerical implementation in MATLAB given.[20]

F. Parameter settings

The domain size is chosen to be $L = 4\pi$. The critical wavenumber which becomes linearly unstable at $r = 0$ is then $k_c = \pm 2$. The size of the spatial grid for the numerical solution is $M = 200$, corresponding to a mesh size $\Delta x = \pi/50$. The time step is $\Delta t = 0.02$; the solution is sampled at sampling interval $\delta t = 5\Delta t = 0.1$. A case without dispersion, $s = 0$, and a case with dispersion, $s = 0.5$, are considered. In the system without dispersion, the eigenvalues of the linear operator are purely real; in the system with dispersion, we have pairs of complex conjugate eigenvalues. These two cases more generally represent two generic behaviors: a system with purely damped modes and a system with oscillatory modes. The noise level is set to $\sigma = 0.01$. Mainly spatially white noise is used, but also a case with spatially colored noise with correlation length $c = 3\pi/2$ is discussed. The bifurcation parameter r is varied within the range [–1, 0.05]. The number of retained principal components is set to $K = 12$ throughout the paper. The results are very insensitive to the choice of K once about 8 principal components are retained.

IV. RESULTS

Prior to the first instability (for $r < 0$), the mean state of the Swift-Hohenberg model is virtually zero and the variance of the system is pretty small, growing close to the bifurcation. A detrending is therefore here not necessary and the linear approximation for the dynamics can be expected to hold to a good degree (cf. Ref. 20) It is natural to compare the reconstructed eigenvalues and eigenvectors of the POP model with those of the linear operator of the system.

A. Stationary data

We start with analysis of stationary datasets and an investigation of the quality of eigenvalue and eigenvector reconstruction in this setting. For both cases $s = 0$ and $s = 0.5$, sample integrations of the full nonlinear stochastic Swift-Hohenberg model are performed for the values $r = -1$, $r = -0.25$, $r = -0.05$ and $r = 0.05$, representing the approach to and passage through the first bifurcation of the homogeneous state $u = 0$. The integrations extend over the time window [0, 1000]; the length of the time series is $N = 10\,000$.

Figure 1 displays parts of these datasets for $s = 0$. The solutions are dominated by wavenumbers $k = \pm 2$ as the least stable modes; the timescale of the system visibly increases when approaching the bifurcation. After the Turing bifurcation, there is a large-amplitude stationary wave solution of wavenumber 2.

The solutions of the system in the case $s = 0.5$ are shown in Fig. 2. Again, the recovery timescale of the system clearly increases when approaching the bifurcation. At $r = -0.05$, the emerging traveling wave pattern is already visible. After the Hopf bifurcation, there is a large-amplitude traveling wave solution. The period of the nonlinear solution is

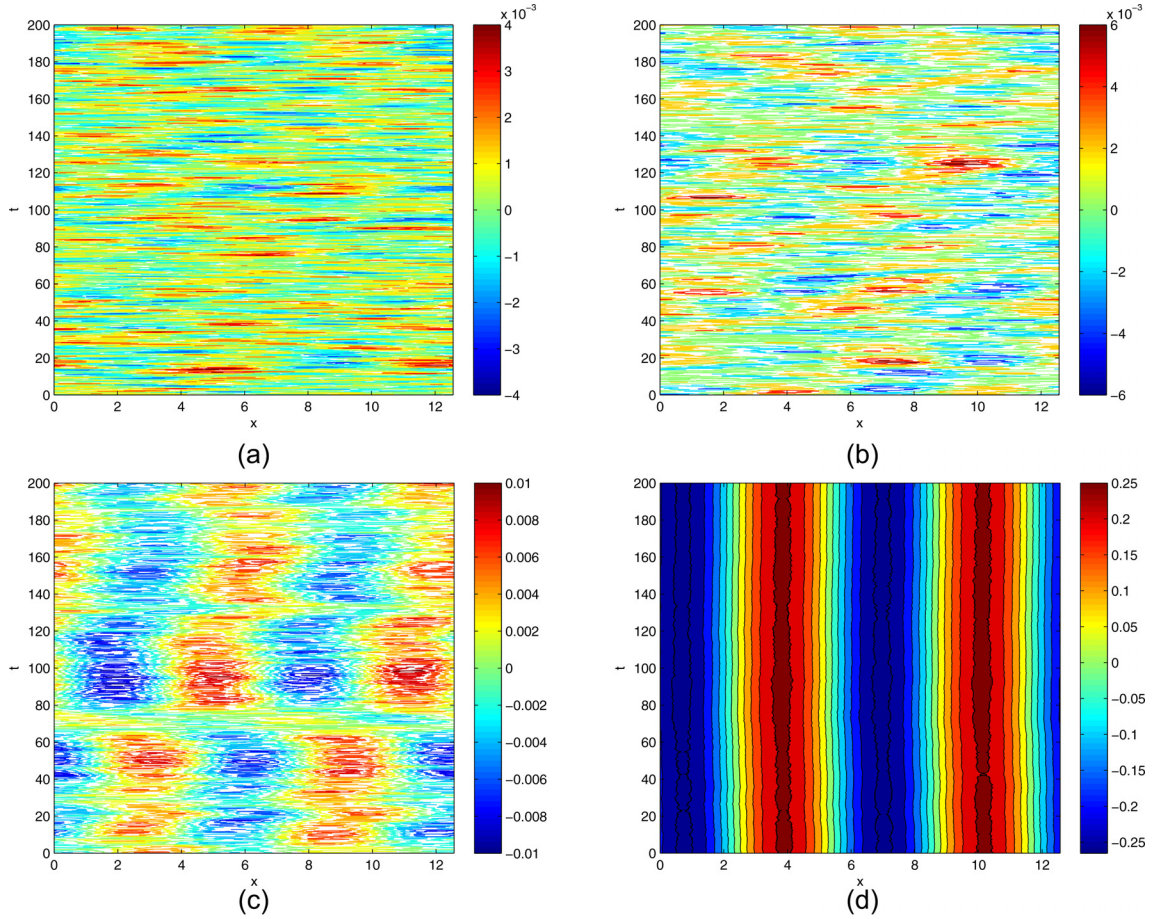

FIG. 1. Sample integrations of the stochastic Swift-Hohenberg model for $s=0$ and $r=-1$ (a), $r=-0.25$ (b), $r=-0.05$ (c), and $r=0.05$ (d).

actually very close to the period obtained from linear theory which is $2\pi/s=4\pi$.

Figure 3 shows the four leading eigenvalues of the linear operator of the system and those reconstructed with the discrete and continuous POP models for the case without dispersion. The eigenvalues are purely real; the third least stable eigenvalue is single, the others are double. The critical (double) eigenvalue is $\alpha_c=r$. Overall, the reconstruction is very good. Expectedly, errors are larger for the more strongly damped modes with the discrete POP model performing better on them than the continuous POP model. The degenerate situation of double eigenvalues is reconstructed as two slightly different eigenvalues. For $r=-1$, one of the double eigenvalues is reconstructed as a complex conjugate pair with almost zero frequency.

For the model with dispersion, the leading eigenvalues are a single real eigenvalue and three complex conjugate pairs (Fig. 4). The critical eigenvalues are $\alpha_c=r\pm is$. Again, the reconstruction of the eigenvalue spectrum of the system from the datasets is very accurate, particularly for the least stable modes. The estimation method using the discrete POP model is somewhat better than that using the continuous POP model.

We now look at the extracted POP modes of the system. Figure 5 displays the first seven POPs for the case $r=-0.05$ and $s=0$ using the discrete POP model. They correspond to the eigenvalues shown in Fig. 3(c) and are purely real. It is known that the true modes of the system are Fourier modes and from Eq. (43), it can be seen that in order of increasing stability, there are the wavenumbers $k=\pm2$, $k=\pm1$, $k=0$, and $k=\pm3$. Therefore, we look at the decomposition of the POPs in terms of the Fourier modes. The contribution of wavenumbers $\pm k$ to the POP p_j is defined as $\gamma_{0,j}=|(\phi_0,p_j)|^2$ and $\gamma_{k,j}=|(\phi_{-k},p_j)|^2+|(\phi_k,p_j)|^2$ for $k>0$. We have $\sum_k\gamma_{k,j}=1$ for all j. The modes of the system are very well reproduced. In particular, the critical modes p_1 and p_2 almost perfectly span the space of ϕ_2 and ϕ_{-2}. There are small errors in the other POPs. The POPs extracted with the continuous POP model (not shown) are very close to the POPs from the discrete POP model.

Figure 6 displays the results for the model with dispersion ($s=0.5$). The POPs correspond to the eigenvalues shown in Fig. 4(c). The modes from the discrete POP model are shown. There are the complex conjugate pairs p_1 and p_2, p_3 and p_4, the real mode p_5, and the complex conjugate pair p_6 and p_7. The critical modes are perfectly reproduced; there are small distortions in the other modes. Again, the results from the continuous POP model (not shown) are almost identical.

We also look at the system driven by spatially colored rather than spatially white noise. Figure 7 displays the case close to the bifurcation ($r=-0.05$) without and with dispersion. The reconstruction of the eigenvalue spectrum of the system from the datasets is about as good as for spatially

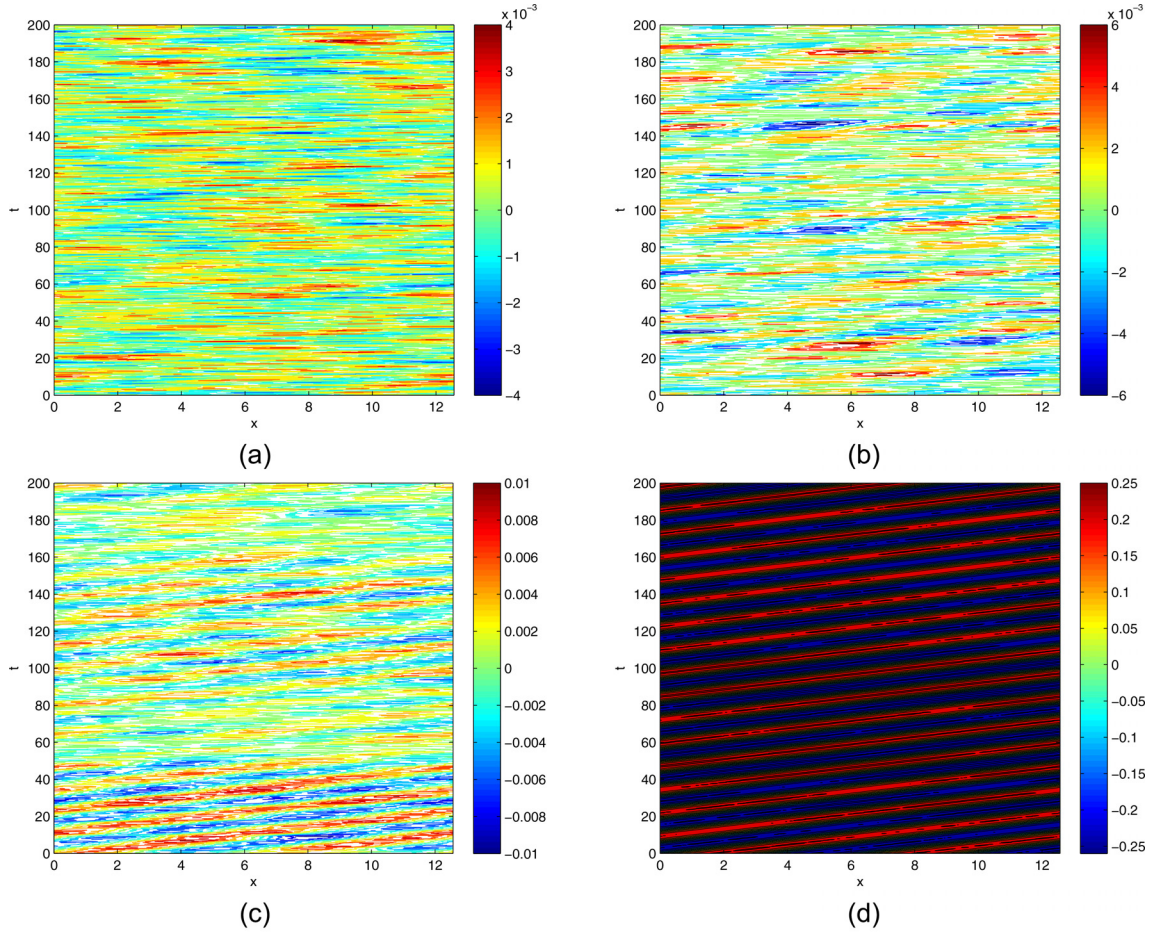

FIG. 2. Sample integrations of the stochastic Swift-Hohenberg model for $s = 0.5$ and $r = -1$ (a), $r = -0.25$ (b), $r = -0.05$ (c), and $r = 0.05$ (d).

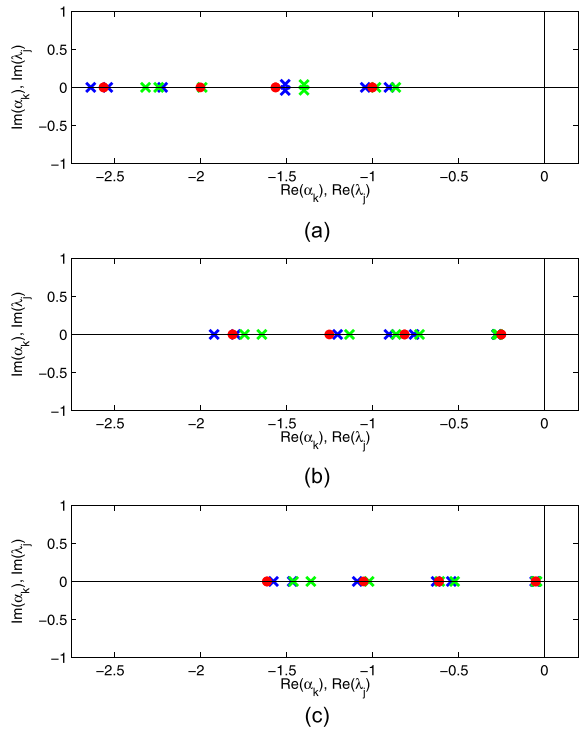

FIG. 3. Eigenvalues of the linear operator of the Swift-Hohenberg equation (red), and eigenvalues reconstructed with the discrete POP model (blue) and the continuous POP model (green) for $s = 0$ and $r = -1$ (a), $r = -0.25$ (b), and $r = -0.05$ (c).

white noise. We also looked at the spatial structure of the POP modes (not shown). The spatially colored noise excites the wavenumbers 0 and ± 1 more strongly than the spatially white noise does. Therefore, these wavenumbers gain more variance in the system than they do for spatially white noise which makes the pattern extraction problem harder. The errors are larger than for white noise, as there is some mixing between the wavenumbers, but the leading modes are still very well identified with contributions of wavenumber 2 well above 0.95.

The conclusions drawn from single integrations of the model are confirmed in an ensemble of 20 such simulations (not shown). Particularly, the critical eigenvalues and modes are reliably identified with small errors as the system approaches the bifurcation and the timescale of the critical modes separates more clearly from the timescales of the other modes. This is encouraging, as it is *a priori* not clear how good the linear approximation still is when the variance of the system grows close to the transition.

B. Sliding window approach

We now examine nonstationary datasets. Integrations of the stochastic Swift-Hohenberg model are performed over the time interval [0, 2000] in which the bifurcation parameter r is linearly ramped as $r(t) = -1 + t/2000$. The integrations start with $r = -1$ at $t = 0$ and reach the bifurcation ($r = 0$) at

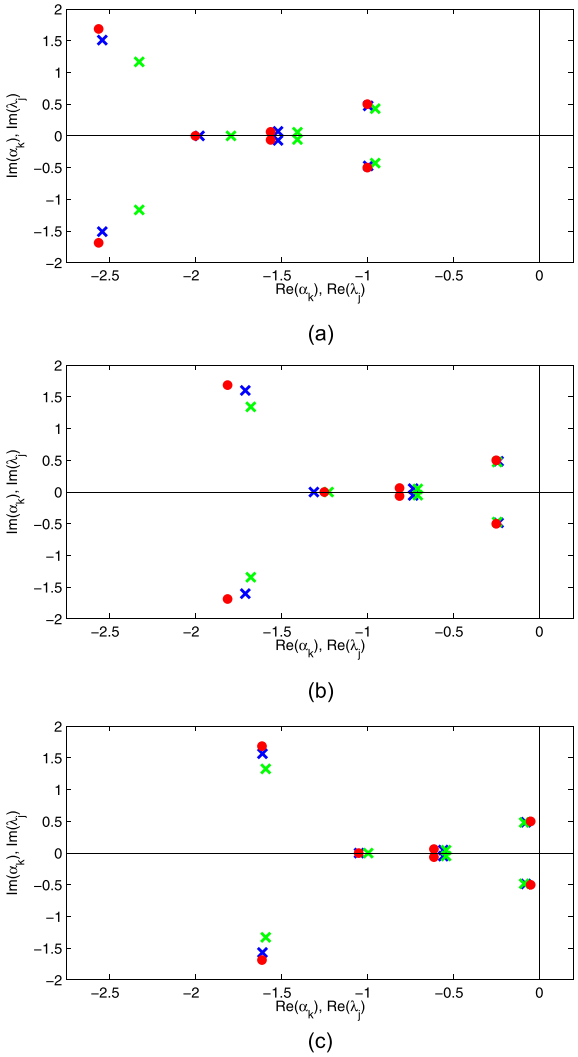

FIG. 4. Eigenvalues of the linear operator of the Swift-Hohenberg equation (red), and eigenvalues reconstructed with the discrete POP model (blue) and the continuous POP model (green) for $s = 0.5$ and $r = -1$ (a), $r = -0.25$ (b), and $r = -0.05$ (c).

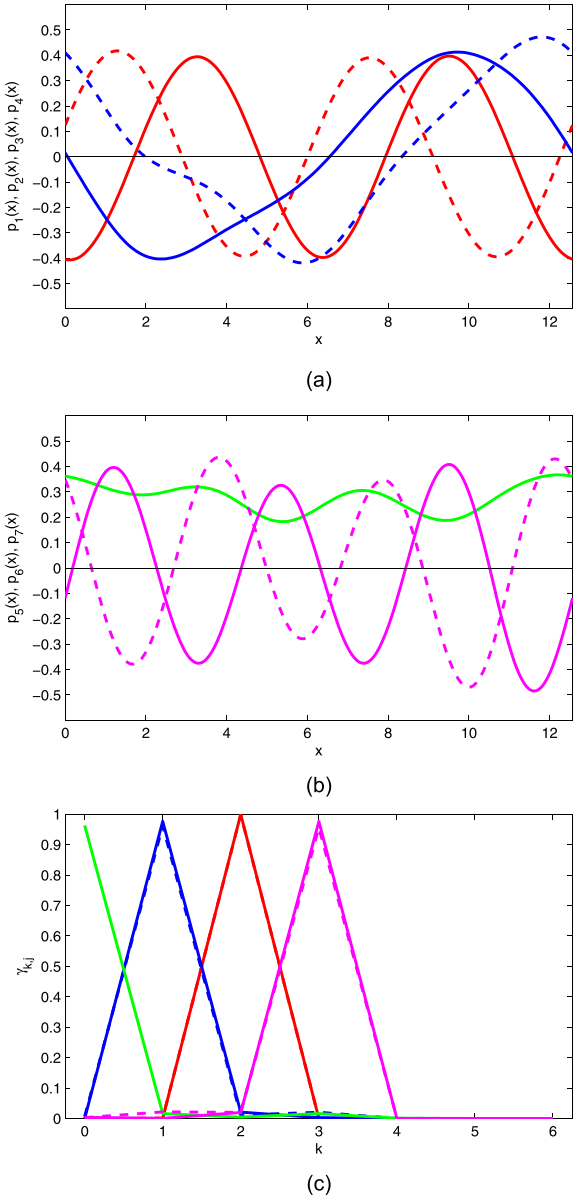

FIG. 5. (a) First (red solid), second (red dashed), third (blue solid), and fourth (blue dashed) POP. (b) Fifth (green), sixth (magenta solid), and seventh (magenta dashed) POP. (c) Contribution of wavenumbers to the POPs. Parameter setting is $r = -0.05$ and $s = 0$.

$t = 2000$. The length of the time series is 20001. The two different sliding window sizes $T_w = 250$ and $T_w = 400$ are considered; they correspond to $N = 2500$ and $N = 4000$, respectively.

Figure 8(a) displays the real part of the least stable eigenvalue of the system as a function of the end of the sliding window for $s = 0$. The true critical eigenvalue is $\alpha_c(t) = r(t)$. The POP analysis tracks the changing stability of the system toward the bifurcation very well. Expectedly, the reconstruction lags behind the true values as data from the past are used for the analysis. This effect is more severe for the larger window length. On the other hand, the statistical sampling fluctuations are larger with the shorter window length, as fewer data points are used for the analysis. The sampling fluctuations become smaller as the system comes closer to the bifurcation because the timescale of the critical modes then separates more clearly from the timescales of the other modes. The results for the discrete and the continuous POP model are very close to each other.

Figures 8(b) and 8(c) show the real and imaginary part of the critical eigenvalue extracted with the POP analysis for the case $s = 0.5$. The true critical eigenvalues here are $\alpha_c(t) = r(t) \pm is$. Again, the changing stability of the system is tracked very well with some time lag. The statistical sampling fluctuations appear to be smaller than for $s = 0$. This may be due to the fact that there is more information in the data, as the non-zero frequency constrains the model inference more strongly. Also the frequency of the critical mode can be extracted from the data with the POP analysis. We observe some error and large sampling fluctuations initially. The results from the discrete and the continuous POP model differ more significantly than for the real part of the eigenvalue. But all the methods appear to converge as the system comes closer to the bifurcation and the frequency of the emerging traveling wave solution is correctly anticipated.

Figure 9 displays summary information from an ensemble of 50 simulations for the discrete POP model. The ensemble

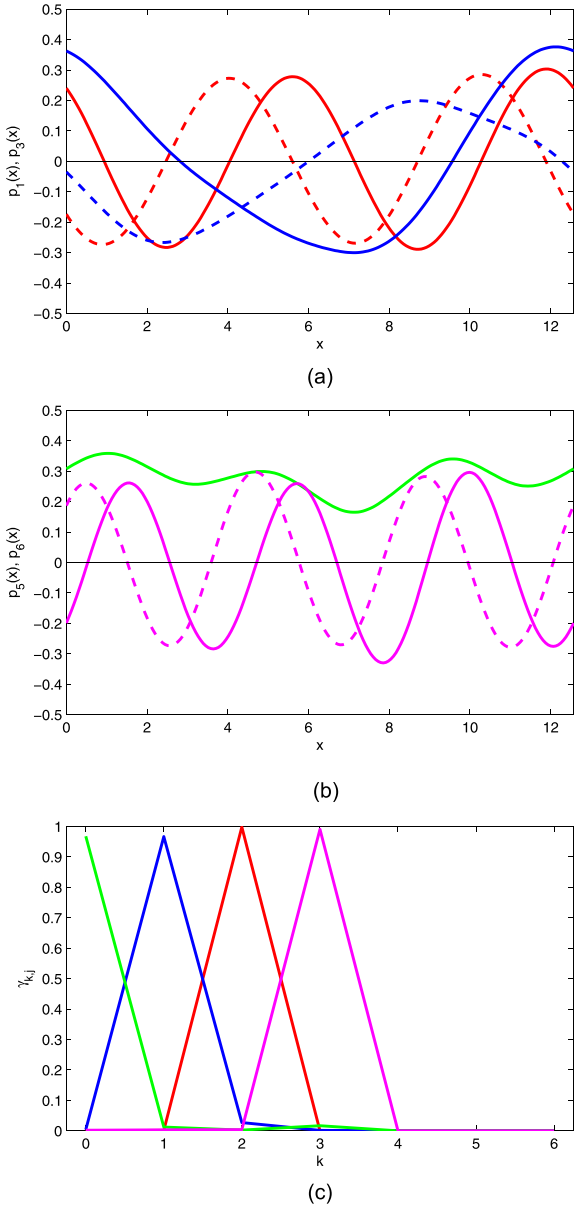

FIG. 6. (a) First POP (red, real part solid, imaginary part dashed) and third POP (blue, real part solid, imaginary part dashed). (b) Fifth POP (green) and sixth POP (magenta, real part solid, imaginary part dashed). (c) Contribution of wavenumbers to the POPs. Parameter setting is $r=-0.05$ and $s=0.5$.

mean steadily tracks the real part of the true critical eigenvalue with some time lag. For the imaginary part of the critical eigenvalue, the ensemble mean fluctuates with small amplitude around the true value, consistent with an unbiased estimation. The standard deviation of all the quantities decreases as the transition point is approached. It is smaller for the system with dispersion in accordance with the observation in Fig. 8.

In order to check whether also the spatial structure of the critical mode of the system is correctly identified, we look at the contribution of wavenumber ± 2 to the least stable POP mode (Fig. 10). Over the whole course of the integration, a large contribution of wavenumber ± 2 to the critical mode is robustly extracted. Some sampling fluctuations are observed initially, in particular, with the shorter window length. As the system approaches the bifurcation, the spatial structure of the critical mode is almost perfectly

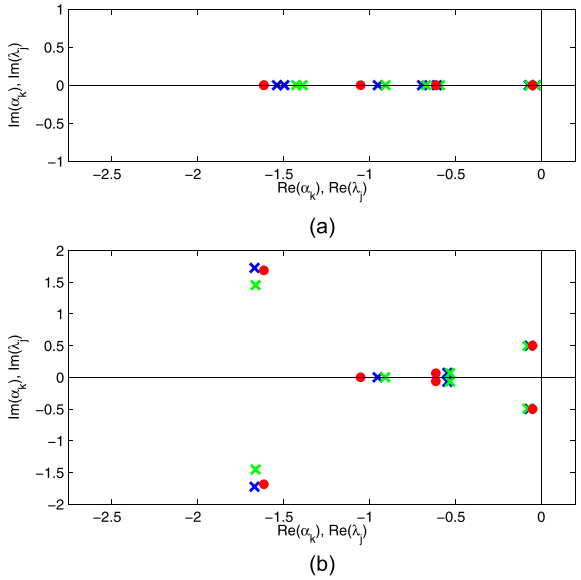

FIG. 7. Spatially correlated noise: eigenvalues of the linear operator of the Swift-Hohenberg equation (red), and eigenvalues reconstructed with the discrete POP model (blue) and the continuous POP model (green) for $r=-0.05$ and $s=0$ (a) and $s=0.5$ (b).

and very robustly identified; this is especially true for the model with dispersion ($s=0.5$). The results from the discrete and the continuous POP model are almost identical here.

Figure 11 gives the corresponding summary information from the ensemble of simulations for the discrete POP model. It confirms an improvement of the reconstruction as the system comes closer to the bifurcation point. The reconstruction is more accurate with the larger sliding window length and for the system with dispersion.

For the integrations with the ramped bifurcation parameter r, we also look at more conventional early-warning signs. A generic early-warning sign for critical transitions is increasing autocorrelation (critical slowing down), here measured by the spatially averaged lag-1 autocorrelation

$$R=\frac{1}{M}\sum_{j=0}^{M-1}\frac{\sum_{n=0}^{N-1}\left[u(x_j,t_n)-\langle u(x_j)\rangle\right]\left[u(x_j,t_{n+1})-\langle u(x_j)\rangle\right]}{\sum_{n=0}^{N}\left[u(x_j,t_n)-\langle u(x_j)\rangle\right]^2}, \tag{54}$$

with

$$\langle u(x_j)\rangle=\frac{1}{N+1}\sum_{n=0}^{N}u(x_j,t_n). \tag{55}$$

The autocorrelation in the system is clearly increasing toward the bifurcation both for $s=0$ and $s=0.5$ (Fig. 12). The autocorrelation is larger for the shorter sliding window as the effect of lagging behind is less severe. There is a clear correspondence here between the rising spatially averaged autocorrelation and an eigenvalue approaching criticality; both quantities carry very similar information. But the spatially averaged autocorrelation does not reveal as much information about the underlying dynamics as the POP

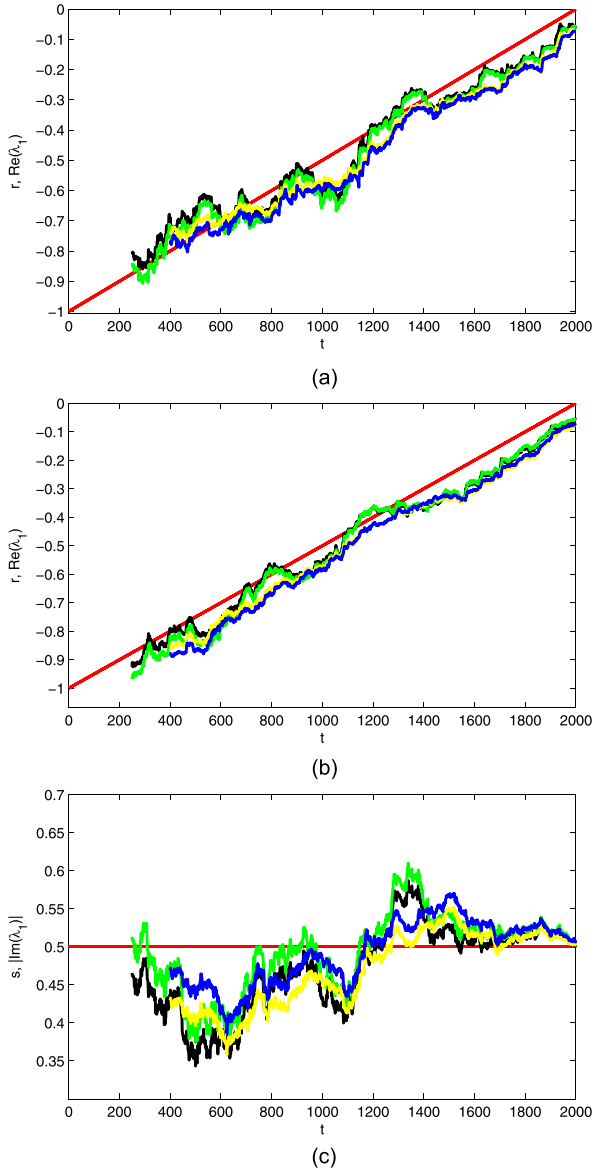

FIG. 8. (a) Real part of the least stable eigenvalue for $s=0$. (b) Real part of the least stable eigenvalue for $s=0.5$. (c) Imaginary part of the least stable eigenvalue for $s=0.5$. Two sliding window lengths are used: $T_w=250$ (green – discrete POP model, black – continuous POP model) and $T_w=400$ (blue – discrete POP model, yellow – continuous POP model). The red solid lines indicate the true values.

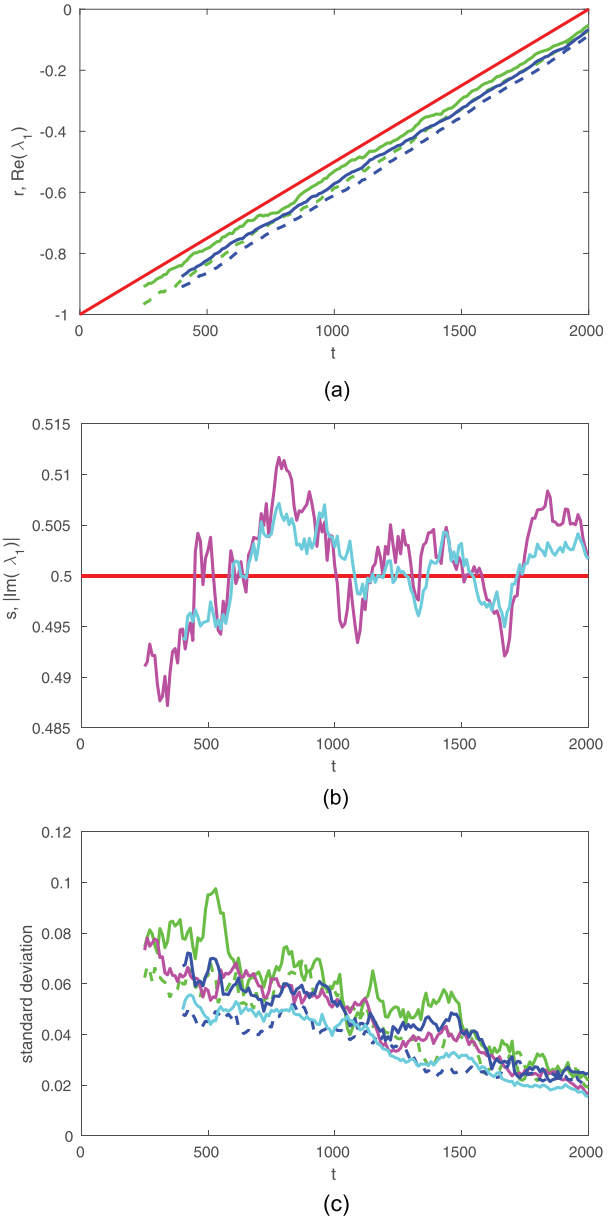

FIG. 9. Ensemble of 50 simulations: (a) Mean real part of the least stable eigenvalue for $s=0$ (solid) and $s=0.5$ (dashed). Two sliding window lengths are used: $T_w=250$ (green) and $T_w=400$ (blue). The red solid line indicates the true value. (b) Mean imaginary part of the least stable eigenvalue for $s=0.5$ and two sliding window lengths: $T_w=250$ (magenta) and $T_w=400$ (cyan). The red solid line indicates the true value. (c) Standard deviation of the various quantities over the ensemble. Color coding is the same as in panels (a) and (b).

analysis, for example, the spatial pattern associated with the instability. Also, another generic early-warning sign, increasing variance, both spatially averaged temporal variance and temporally averaged spatial variance, is present in the Swift-Hohenberg model.[20]

One may try to derive more quantitative and specific information from indicators such as increasing autocorrelation and increasing variance by looking at scaling laws for them as a function of the distance from the instability threshold.[1,20] However, it may turn out that such scaling laws break down as the bifurcation is approached because the linear approximation is not sufficiently valid any more for them to hold.[20]

Generally it is recommended to always perform the sliding window analysis for several choices of the window length T_w and to look for consistency in the results. There is always a trade-off between the size of the statistical sampling fluctuations and the reconstruction lag. For the present system, the smallest useful window size is about $T_w=150$. A possible approach to reducing the reconstruction lag might lie in using a weighting scheme in the sliding window which weights the most recent observations more strongly.

C. Nonstationary POP analysis

We now explore the nonstationary POP analysis. The same integrations described before with the linearly ramped bifurcation parameter r varied as $r(t)=-1+t/2000$ are used. They extend on the time interval [0, 2000] and reach the bifurcation point at $t=2000$. A learning data window is

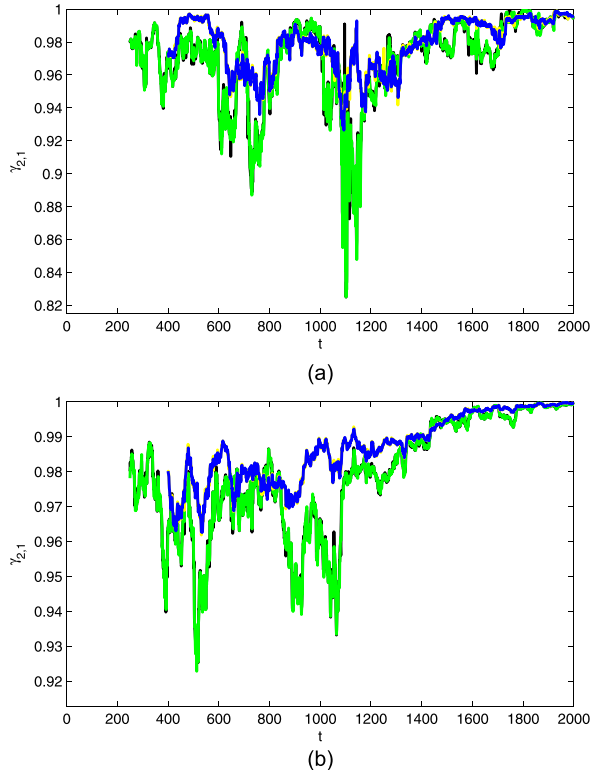

FIG. 10. Contribution of wavenumber 2 to the least stable POP mode for $s=0$ (a) and $s=0.5$ (b). Two sliding window lengths are used: $T_w=250$ (green – discrete POP model, black – continuous POP model) and $T_w=400$ (blue – discrete POP model, yellow – continuous POP model).

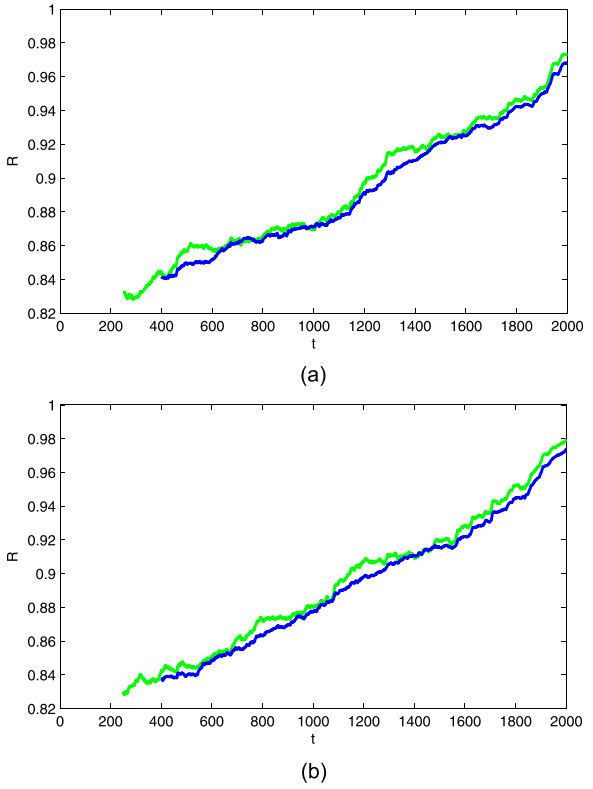

FIG. 12. Spatially averaged lag-1 autocorrelation R for $s=0$ (a) and $s=0.5$ (b). Two sliding window lengths are used: $T_w=250$ (green) and $T_w=400$ (blue).

defined as $[0, t_e]$ where the end point t_e is varied on the interval [800, 2000]. For each value of t_e, a nonstationary POP analysis is performed as introduced in Sec. II which then allows to reconstruct the system on the learning data window $[0, t_e]$ and to predict it beyond t_e. We use a discrete POP model with a linear trend

$$\mathbf{B}(t) = \mathbf{B}_0 + t\mathbf{B}_1. \tag{56}$$

Figure 13 displays the reconstructed/predicted real part of the least stable eigenvalue of the system for $s=0$ and $s=0.5$. The areas below the solid black lines refer to reconstruction (target time smaller than t_e); the areas above the solid black lines refer to prediction (target time larger than t_e). In statistics, this is often referred to as in sample and out of sample. If t_e is too small the reconstruction/prediction is not very robust. With $s=0$. the results stabilize at about $t_e=1100$ with a slight overprediction of instability and they become very good from about $t_e=1450$. With $s=0.5$, the reconstruction and prediction is very robust and accurate from about $t_e=1200$. The results with a continuous POP model are almost indistinguishable (not shown).

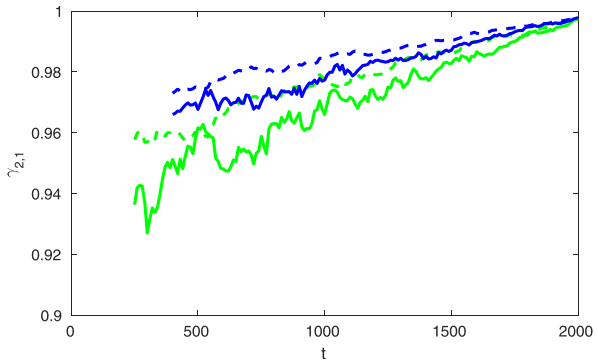

FIG. 11. Ensemble of 50 simulations: Mean contribution of wavenumber 2 to the least stable POP mode for $s=0$ (solid) and $s=0.5$ (dashed). Two sliding window lengths are used: $T_w=250$ (green) and $T_w=400$ (blue).

Figure 14 displays summary statistics on the nonstationary POP analysis from an ensemble of 100 simulations. Panel (a) shows the predicted bifurcation time, that is, the time when an unstable eigenvalue occurs in the nonstationary POP model. On average, the bifurcation time is well predicted. There is some delay in the system with dispersion which decreases with increasing learning window size. The fluctuations in the predictions markedly decrease with increasing learning window size. Panel (b) gives the contribution of wavenumber 2 to the leading POP mode. The reconstruction improves with increasing learning window size; beyond about $t_e=1500$, it is very reliable. Identification is better for the system with dispersion; in particular, very bad reconstructions occur less frequently.

A possible way to reduce the variability in the predictions might be to take into account parameter uncertainty which may be substantial here given the large number of parameters in the nonstationary model. The likelihood-based framework gives access to uncertainty information via the Fisher information matrix. Each prediction would be formed as an average over an ensemble generated by sampling from the parameter error distribution. A similar technique has been used for nonstationary probability density modelling.[12]

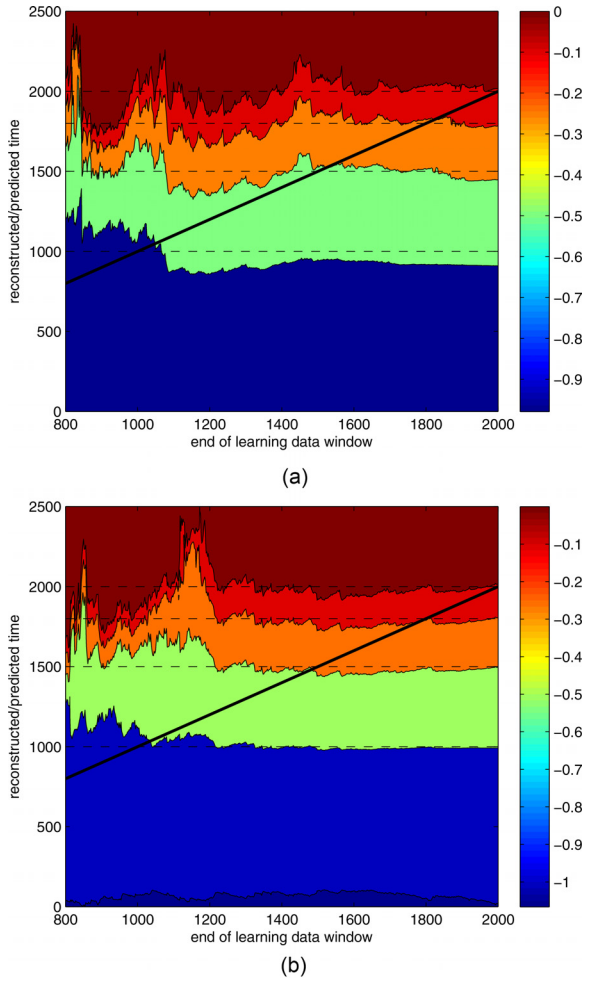

FIG. 13. Real part of the least stable eigenvalue as a function of the end of the learning data window for $s=0$ (a) and $s=0.5$ (b). Dashed horizontal lines indicate the true eigenvalue and, from bottom to top, refer to the values -0.5, -0.25, -0.1, and 0 (bifurcation point). The color contours refer to the same values. The solid black line separates reconstruction from prediction.

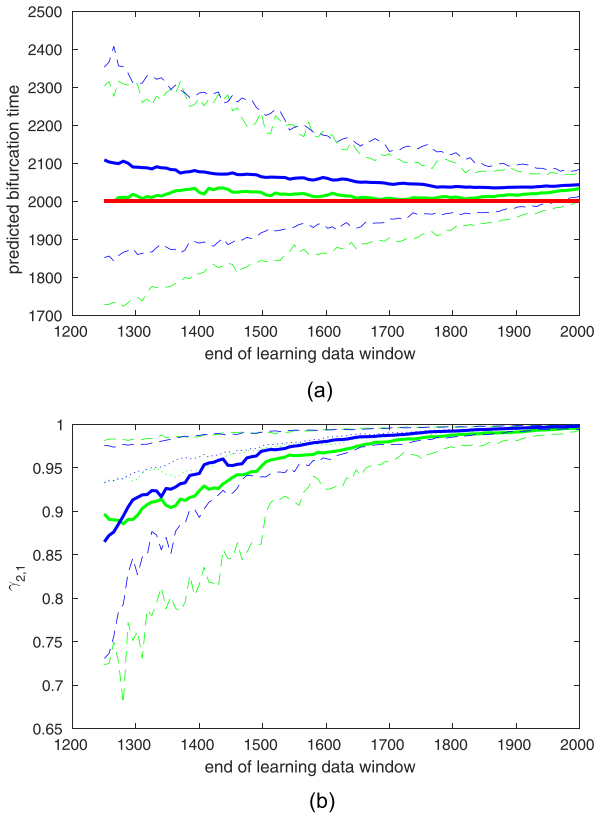

FIG. 14. Ensemble of 100 simulations: (a) Predicted bifurcation time for $s=0$ (green) and $s=0.5$ (blue). The solid lines indicate the mean over the ensemble, the dashed lines the 10% and 90% quantiles of the ensemble. The red solid line indicates the true value. (b) Contribution of wavenumber 2 to the least stable POP mode for $s=0$ (green) and $s=0.5$ (blue). Solid lines indicate the mean over the ensemble, dashed lines the 10% and 90% quantiles, and dotted lines, the 50% quantile.

V. DISCUSSION AND CONCLUSIONS

A data-driven methodology for detecting, anticipating, and predicting critical transitions in spatially extended systems based on POP analysis was introduced. The system is approximated by a linear stochastic dynamical system and the principal modes and their stability properties are extracted from data. The technique was explored using nonlinear integrations of the one-dimensional stochastic Swift-Hohenberg model.

When applied to stationary datasets produced at different values of the bifurcation parameter, the method is able to reconstruct the principal eigenvalue spectrum of the system as well as the spatial structure of the corresponding modes. The reconstruction of the critical eigenvalue and mode is particularly good.

The method was then applied to nonstationary datasets using a sliding window approach. It was able to track the linear stability properties of the system and anticipate the impending bifurcation. The characterization of the critical mode is particularly reliable and improves when the system comes closer to the bifurcation point. This is in contrast to recently considered scaling laws for autocorrelation and variance which may break down close to the bifurcation point.[20]

A genuinely nonstationary POP analysis was introduced based on the explicit inference of the nonstationarity using a nonautonomous linear dynamical system. It is capable of predicting the timing of the transition well ahead of the bifurcation point.

The present technique makes a more detailed use of the available spatio-temporal data than summary statistics such as spatially averaged autocorrelation and temporal or spatial variance and thus extracts more specific information, directly linked to the underlying dynamics. Yet, the POP analysis may still be termed generic as a simple and robust time series model is used and no *a priori* knowledge about the underlying system dynamics is required.

The POP analysis is clearly based on the assumption of linear dynamics. Further investigation of its validity in nonlinear systems is necessary. The technique will probably be mainly applicable to the first bifurcation from a homogeneous state to a patterned state as in the present study. When looking, for example, at the opposite direction of control parameter variation, that is, at the supercritical bifurcation from the large-amplitude patterned state to the zero state, a nonlinear model will be necessary.[13]

[1]C. Kuehn, Physica D **240**, 1020 (2011).
[2]H. Held and T. Kleinen, Geophys. Res. Lett. **31**, L23207, https://doi.org/10.1029/2004GL020972 (2004).

[3]V. Dakos, M. Scheffer, E. H. van Nes, V. Brovkin, V. Petoukhov, and H. Held, Proc. Natl. Acad. Sci. U.S.A. **105**, 14308 (2008).
[4]S. R. Carpenter and W. A. Brock, Ecol. Lett. **9**, 311 (2006).
[5]M. Scheffer, J. Bascompte, W. A. Brock, V. Brovkin, S. R. Carpenter, V. Dakos, H. Held, E. H. van Nes, M. Rietkerk, and G. Sugihara, Nature **461**, 53 (2009).
[6]V. Guttal and C. Jayaprakash, Ecol. Lett. **11**, 450 (2008).
[7]V. N. Livina, F. Kwasniok, and T. M. Lenton, Clim. Past **6**, 77 (2010).
[8]V. N. Livina, F. Kwasniok, G. Lohmann, J. W. Kantelhardt, and T. M. Lenton, Clim. Dyn. **37**, 2437 (2011).
[9]J. M. T. Thompson and J. Sieber, IMA J. Appl. Math. **76**, 27 (2011).
[10]W.-X. Wang, R. Yang, Y.-C. Lai, V. Kovanis, and C. Grebogi, Phys. Rev. Lett. **106**, 154101 (2011).
[11]C. L. E. Franzke, Physica D **262**, 35 (2013).
[12]F. Kwasniok, Phys. Rev. E **88**, 052917 (2013).
[13]F. Kwasniok, Phys. Rev. E **92**, 062928 (2015).
[14]M. S. Williamson and T. M. Lenton, Chaos **25**, 036407 (2015).
[15]V. Dakos, S. Kefi, M. Rietkerk, E. H. van Nes, and M. Scheffer, Am. Nat. **177**, E153 (2011).
[16]V. Dakos, E. H. van Nes, R. Donangelo, H. Fort, and M. Scheffer, Theor. Ecol. **3**, 163 (2010).
[17]R. Donangelo, H. Fort, V. Dakos, M. Scheffer, and E. H. van Nes, Int. J. Bifurcation Chaos **20**, 315 (2010).
[18]V. Guttal and C. Jayaprakash, Theor. Ecol. **2**, 3 (2009).
[19]S. Kéfi, M. Rietkerk, C. L. Alados, Y. Peyo *et. al*., Nature **449**, 213 (2007).
[20]K. Gowda and C. Kuehn, Commun. Nonlinear Sci. Numer. Simul. **22**, 55 (2015).
[21]K. Hasselmann, J. Geophys. Res. **93**, 11015, https://doi.org/10.1029/JD093iD09p11015 (1988).
[22]H. von Storch, G. Burger, R. Schnur, and J.-S. Von Storch, J. Clim. **8**, 377 (1995).
[23]P. J. Schmid, J. Fluid Mech. **656**, 5 (2010).
[24]I. T. Jolliffe, *Principal Component Analysis* (Springer, 2010).
[25]J. Swift and P. C. Hohenberg, Phys. Rev. A **15**, 319 (1977).
[26]M. C. Cross and P. C. Hohenberg, Rev. Mod. Phys. **65**, 851 (1993).
[27]J. Burke, S. M. Houghton, and E. Knobloch, Phys. Rev. E **80**, 036202 (2009).
[28]P. E. Kloeden and E. Platen, *Numerical Solution of Stochastic Differential Equations* (Springer, 2010).
[29]J. Garcia-Ojalvo and J. Sancho, *Noise in Spatially Extended Systems* (Springer, 1999).